Deep Resources Engineering 2 (2025) 100198

Contents lists available at ScienceDirect

Deep Resources Engineering

journal homepage: www.keaipublishing.com/en/journals/deepre/

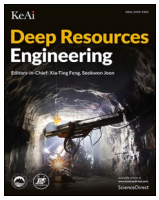

Full length article

Fracture mechanism of tunnel surrounding rock induced by blasting disturbances: Experiments and numerical simulations

Jianpo Liu [a,*], Fengtian Li [a], Xiaonan Wang [b], Yingtao Si [a], Yandi Fan [a], Zixuan Zhang [a], Yongxin Wang [a]

[a] State Key Laboratory of Intelligent Deep Metal Mining and Equipment, Northeastern University, Shenyang 110819, China
[b] Benxi Longxin Mining Co., Ltd, Benxi 117013, China

ARTICLE INFO

Keywords:
Blasting disturbance
Tunnel
Fracture mechanism
RA-AF
Block discrete element

ABSTRACT

The inversion of the source mechanism is a critical step in revealing and understanding the mechanisms of rock mass failure and guiding the prevention and control of ground pressure disasters. Under conditions of high stress and strong blasting disturbances, the formation, clustering, and interconnection of internal cracks in the surrounding rock of tunnels are highly likely to induce rock mass failure. Investigating the failure mechanisms of tunnel surrounding rock induced by strong blasting disturbances is essential for achieving effective tunnel protection. In this study, acoustic emission (AE) monitoring technology was employed to capture micro-fracture signals from the surrounding rock in real time. The RA-AF ratio method was utilized to classify crack types, while discrete element numerical simulations were conducted to analyze crack propagation patterns under dynamic disturbances. The results indicate that tensile-type cracks dominate during the static stress-controlled stage of tunnel failure, whereas blasting disturbances significantly accelerate shear crack propagation. Stress waves traveling in different directions produce tensile reflection effects in straight wall regions, leading to the interconnection of shallow cracks on the blast-facing side and the formation of macroscopic fracture zones. Based on these findings, optimization strategies for support design are proposed. Radial constraints should be enhanced on the blast-facing side to suppress shallow surrounding rock deformation, and support depth should be extended along principal stress directions to mitigate rock mass damage and diffusion caused by blasting disturbances.

1. Introduction

For underground engineering rock masses, rock mass failure induced by dynamic disturbance is accompanied by changes in multisource state information, such as stress, deformation, fracture and vibration velocity [1–5]. Academician Gu Jincai et al. built a medium-scale geotechnical anti-explosive physical modeling device that can carry out indoor simulations of conventional explosions on underground engineering penetration induced by the direct impact of the deep engineering damage effect and carried out different forms of charge anti-explosive modeling tests, revealing the effect of different types of support on the crack-blocking effect [6,7]. Tao et al. used a Hopkinson bar to study the dynamic—static coupling test of granite with prefabricated holes and analyzed the failure law of holes induced by stress disturbance under different prestress levels [8]. Based on a similar physical model experiment, Qiu et al. conducted a study on the characteristics of tunnel failure induced by blasting, analyzed the propagation law of blasting stress waves within the sample and the law of strain field on the tunnel surface, and revealed the tensile failure effect caused by blasting stress waves on the free surface [9]. Yang et al. conducted a study on the interaction mechanism between explosive stress waves and cracks, and obtained the variation law of the local stress field at the crack tip under the action of explosive stress waves [10]. The energy evolution patterns during coal destabilization and the damage process under various failure modes are obtained by Xue et al. [11]. Compared with the analysis of the apparent information response law of rock masses, the potential failure area can be identified based on the internal fracture response information of rock masses, and targeted support of the failure area can be realized [12–15]. However, when the potential failure mechanisms of rock masses are inconsistent (such as loose failure, strain rockburst and fault slip mine earthquakes), the dominant fracture types are different, and the corresponding support methods need to be suitable. For example, loose failure is dominated by tensile cracks, and fault slip failure is dominated by shear fractures. A certain number of scholars

* Correspondence to: State Key Laboratory of Intelligent Deep Metal Mining and Equipment, Northeastern University, China
E-mail address: liujianpo@mail.neu.edu.cn (J. Liu).

https://doi.org/10.1016/j.deepre.2025.100198
Received 8 March 2025; Received in revised form 5 May 2025; Accepted 20 May 2025
Available online 24 May 2025

have also carried out investigations on the response mechanism of rock masses to blasting disturbances [16–25]. In the actual tunnel support process, it is necessary to clarify not only the potential failure area of the rock mass under the effect of blasting disturbance but also the gestation mechanism and dominant failure mode of rock mass disasters induced by blasting disturbance.

Acoustic emission technology (AE) can continuously and real-time monitor the generation and propagation of microcracks inside the rock [26,27], and locate the failure position. Commonly used methods for inverting rock fracture mechanisms include moment tensor analysis, initial motion amplitude analysis, and the RA/AF value discrimination method. The analysis of the moment tensor provides in-depth information on the fracture process [28–32]. However, this inversion method is influenced by the heterogeneity and anisotropy of the propagation medium in the actual calculation process; at least six sensor channels are needed to capture signals, and there are many calibration parameters, so the inversion program is complicated [33]. Some simple and convenient fracture mechanism analysis methods have been widely applied to analyze fracture mechanisms. This method was applied to the classification of failure types of cement mortar materials earlier in Japan [34]. Based on this method, Ohtsu and Tomoda [35] analyzed the acoustic emission amplitude characteristics of nontensile cracks and other cracks at different failure stages of reinforced concrete. ; Ohno et al. compared and analyzed the results of the moment tensor inversion method and the RA-AF ratio division method for the classification of crack types during the four-point bending test of concrete and found that when the RA-AF ratio was 1:200, the proportions of the two crack types divided by the two methods were similar, which verified the effectiveness of the RA-AF ratio division method [36]. By analyzing the distribution relationship of RA and AF in different loading stages, Liu et al. found that rock damages are caused by tensile and shear cracks, and shear cracks become more obvious with the increase of deviatoric stress [37]. Many studies have demonstrated that pure tensile events have higher frequencies and shorter rise times than shear or mixed events [38,39]. By comparing the characteristics of different parameters of AE signals released by tensile and shear rupture, it was found that the classification of fracture types based on RA and AF is the most reliable [40].

The elastic strain energy released by shear crack is greater than that released by tensile crack. Most of AE signals generated in compression and shear failures that mainly produce shear cracks have low average frequency (AF) values and low peak frequencies. On the contrary, most of AE signals generated in bending and tensile failures that mainly produce tensile cracks have low RA (ratio of rise time to amplitude) and high peak frequencies [41].

Current research on the stability of tunnel surrounding rock predominantly focuses on the mechanical response characteristics induced by the redistribution of mining-induced stress fields. However, a comprehensive and systematic understanding of the dynamic coupling mechanism between blasting disturbance orientation and rock mass fracture mechanisms remains elusive. Notably, in deep metal mines, the tunnel network is influenced by the coordinated operations of multiple mining areas, where the damage evolution process of the surrounding rock occurs under the superposition of blasting stress waves from various directions. A key scientific issue that has not been adequately addressed in existing studies is the significant spatial orientation sensitivity exhibited by fractures in the surrounding rock caused by disturbance waves incident from different directions.

Therefore, indoor experiments using rock-like materials (cement mortar) were conducted to investigate the acoustic emission characteristics of rock mass surrounding tunnels induced by blasting disturbances in various directions. The RA-AF method for acoustic emission signals was employed to invert the failure mechanism of the rock mass around the tunnel, and the spatio-temporal distribution and evolution patterns of tensile and shear cracks under the combined effects of static stress and blasting disturbances were analyzed. Additionally, discrete element simulations were performed to study crack propagation and macroscopic failure modes of the rock mass surrounding tunnels caused by directional blasting disturbances, thereby revealing the relationship between the failure mechanism of the rock mass and the orientation of blasting disturbances. These findings provide a mesoscopic mechanical basis for differentiated support design in deep tunnels and establish a correlation model linking parametric control of blasting direction with dynamic evaluation of rock mass stability. This research holds significant academic value for enhancing the theoretical framework of disaster prevention and control for rock masses surrounding tunnels under blasting disturbances.

2. Spatiotemporal evolution characteristics of the fracture mechanism of tunnel surrounding rock induced by blasting disturbance

2.1. Experiment parameter setting

In this study, a model of a tunnel and blast hole prefabricated on cement mortar material is studied (Fig. 1a,b.), and acoustic emission monitoring technology is used to capture the internal fracture signal of the surrounding rock of a tunnel. Based on the spatial location of microcracks, the temporal and spatial distributions and evolution laws of different types of cracks induced by the combined action of static stress and blasting disturbance are further analyzed.

Specifically, the pre-set strength of the cement mortar is 12 MPa, utilizing cement of grade 325 and quartz sand as the aggregate. The mass ratio of cement, quartz sand, and water is set at 1:5.1:1.1. During the sample preparation process, a vibrating rod is employed to remove entrapped air within the mixture. Subsequently, the prepared samples are cured under room temperature conditions for 28 days. To prevent cracking, the surfaces of the samples are regularly sprayed with water during the curing period. The number of acoustic emission sensors is 17 (Fig. 1c.). The specific design and layout principles can be found in the literature [42].

The sensor employed has a response frequency range of 50–400 kHz. The preamplifier model is 1220A-AST with a gain of 40 dB. Sampling settings include: a sampling frequency of 10 MHz, a sampling length of 5120 points, and a sampling threshold of 45 dB. To ensure effective coupling between the sensor and the sample, Vaseline was applied at the contact interface, and the sensor was securely fixed using a rubber band.

This experiment employed an array of 17 sensors to perform real-time continuous monitoring of acoustic emission (AE) signals generated by internal microfractures within the surrounding rock of the tunnel. To ensure reliable source localization, a minimum of four detection channels is theoretically required. However, the first eight channels registering signal arrivals were utilized to enhance spatial linear localization accuracy through multi-channel triangulation. For rupture mechanism analysis using the RA-AF-Energy method, the initial AE signal exceeding the predefined amplitude threshold was selected as the representative waveform. This criterion ensures temporal consistency with the incipient fracture event while minimizing noise interference from subsequent signals.

The direction of blasting disturbance includes three schemes: roof, sidewall and floor (Fig. 1d) (Fig. 2). The internal tectonic stress of the rock body is often greater than the gravity of the overlying rock body, which makes the main stress of the deep rock body mostly dominated by horizontal stress, so the design of the study side pressure coefficient is 1.6, as shown in Fig. 1e. By detonating the explosives in the blast hole during the specimen loading period, an external dynamic disturbance effect on the surrounding rock of the tunnel is achieved. In this paper, a bottom-sealed steel pipe is placed in the blasthole in advance to reduce the direct impact of the explosive gas and stress waves near the blasthole, as shown in Fig. 1a. In addition, the experiment imposed multiple blasting disturbances until macroscopic cracks appeared in the tunnel. The explosive adopts a coupling charging method, quartz sand is used to fill, and quick-setting cement is used to plug the hole.

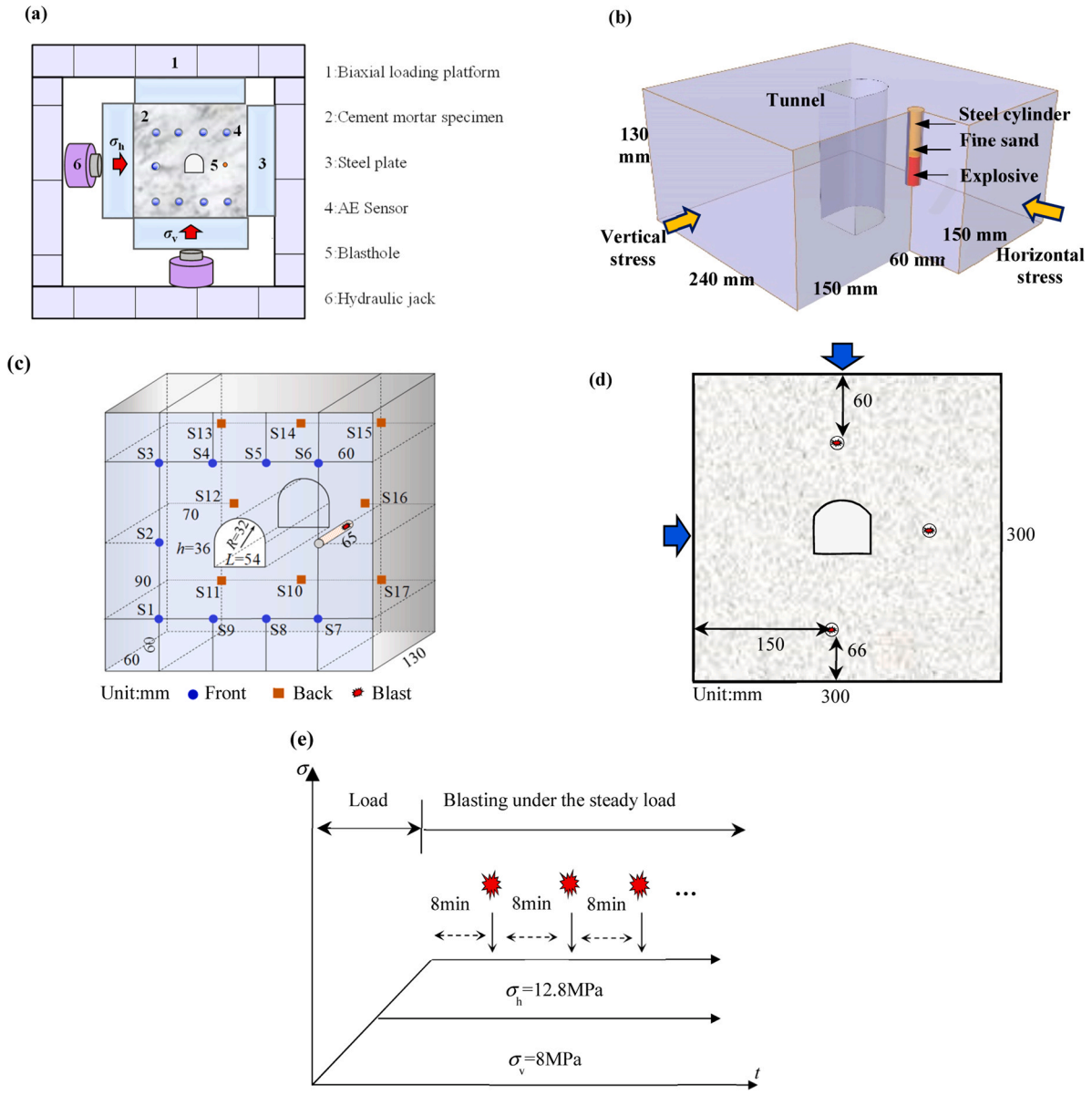

Fig. 1. Experimental model settings: (a) Experiment devices; (b) Model dimension; (c) The layout of the sensors; (d) Charging structure; (e) Static loading path and blast disturbance scheme.

2.2. *Temporal evolution characteristics of acoustic emission signals*

As the stress waves are triggered by high-energy blasting, they may continue to propagate in the specimen for some time. Further,these stress waves may get mixed into the signals that are generated from microcracks. Based on the difference in parameters between signals induced by blasting and microcrack generation and the attenuation law of blasting signals. The simplex method enables high-precision localization of acoustic emission events [43,44].

Given that the sample included a prefabricated tunnel, eight channels that initially received the AE signals without passing through the tunnel holes were selected for localization. During the analysis of fracture mechanisms using the RA-AF-Energy method, the first AE signal exceeding the threshold value was adopted.

In cement-based materials with rich microporous structures, an increase in the propagation distance of elastic waves can cause changes in the acoustic emission signal parameters, such as a decrease in amplitude and an increase in duration, leading to an increase in the shear cracks of microfractures [45,46]. Therefore, when multiple sensors arranged at different positions collect the same waveform signal, differences in the waveform parameters captured by each sensor will occur. To reduce the increase in the RA caused by the increase in the waveform propagation distance, the inversion of rupture types based on first-arrival waveform data has relatively high accuracy [40]. The waveform of the first fracture arrival signal participating in the location is automatically found by writing a MATLAB code, and the RA and AF values of the rupture event are calculated based on this waveform.

Under the coupling effect of principal stress and blast disturbance, the initiation and extension of microfractures in the surrounding rock of a tunnel promote the continuous generation of acoustic emission signals. By plotting the RA and AF values into a two-dimensional density scatter plot, it can be found that the RA generated during the prestress loading stage is mainly distributed in the range of 0–10 ms·V-1, the AF is mainly distributed in the range of 0–200 kHz, the RA in the dense red area is in the range of 0–3 ms·V-1, and the AF is in the range of 20–150 kHz. The results show that the acoustic emission signal parameters are characterized by a shift from the high AF low RA region to the low AF high RA region during the gradual aggravation of the internal damage induced

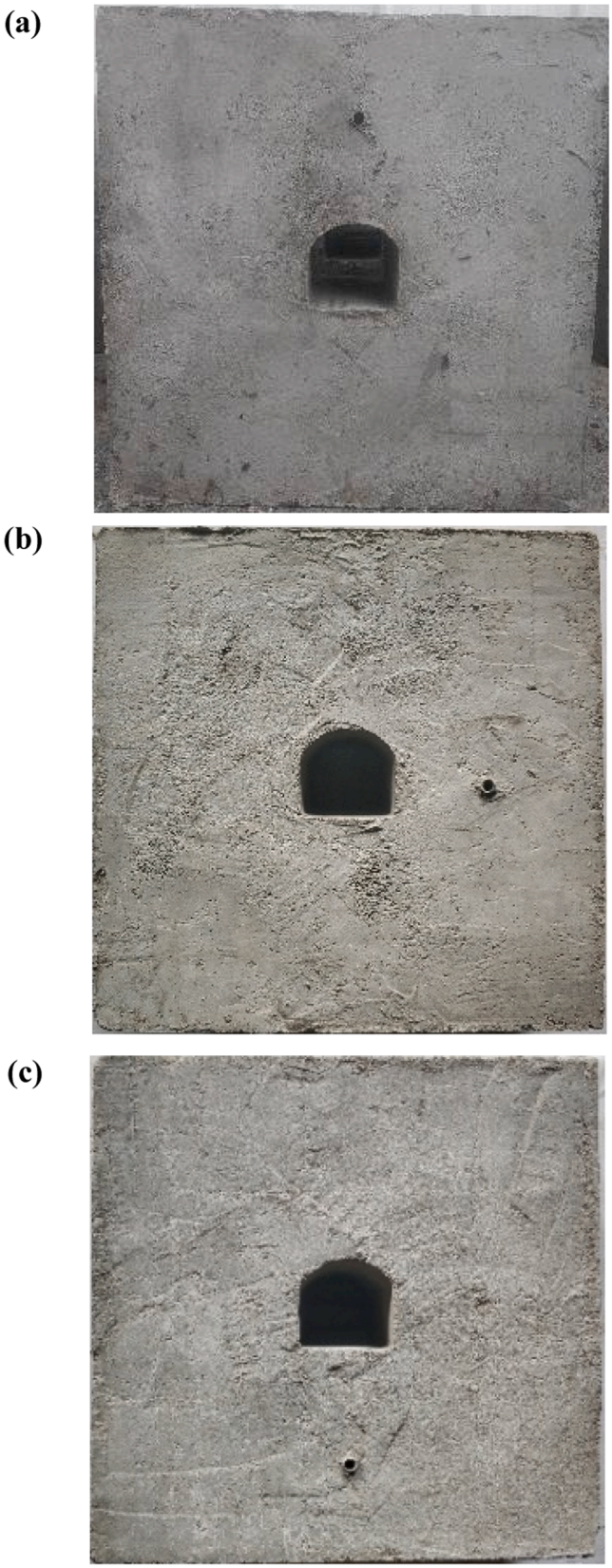

Fig. 2. Model used in tests for different blasting directions: (a) Roof; (b) Right sidewall; (c) Floor.

by the combined effects of static stress and blast disturbance in the rock surrounding the tunnel.

When using the RA-AF discriminant criterion to classify tensile and shear cracks, it is necessary to determine the expression for the basis of discrimination, as shown in Fig. 3. Si et al.[47] proposed a rapid RA-AF-energy rupture type determination method by integrating the variability of energy released from tensile and shear type rupture acoustic emission signals and proposed the basis for the division of different types of cracks within cement mortar, i.e., AF = 9RA+ 66. This criterion is used and plotted in Fig. 4, which shows that the dense red region in the static stress loading phase is located above the transition line, while the dense region of the acoustic emission signal in the blast disturbance phase is shifted to the bottom of the transition line. By counting the number of cracks in different regions in the two stages, it can be found that the microfractures generated in the static stress loading stage are mainly tensile cracks, while the microfractures generated under the blasting disturbance in different directions are mainly shear cracks. For example, when the direction of blasting disturbance is on the roof, the proportions of shear cracks in the pre-stressed loading and blasting disturbance stages are 45.9 % and 74 %, respectively; when the blasting disturbance is on the right side of the tunnel, the proportions of shear cracks produced in the two stages are 46.5 % and 41.9 %, respectively; and when the blasting disturbance is on the floor, the proportions of two-stage shear cracks are 28 % and 53.5 %, respectively.

Based on the proportions of tensile and shear cracks generated by different schemes of static stress loading and blasting disturbance, it can be seen that the blasting disturbance induced tunnel damage in the process of gradual expansion, and cracks from the compression density and linear elasticity stage of the stable expansion stage gradually evolved into a plastic deformation stage in which the cracks of the unstable expansion of the damage zone expansion of the induced mechanism undergo a "tensile—shear" mode change. The expansion-inducing mechanism of the damage zone undergoes a tensile—shear mode shift. In the initial stage of bidirectional stress loading, the whole sample is in a state of compression, the internal microcracks are compacted and gradually close to each other, the relative sliding failure between particles decreases, and the tensile fracture is relatively high. When the stress level inside the rock gradually increases, elastic—plastic deformation and volume expansion begin to occur inside, microfractures gradually start to expand and gradually penetrate, relative dislocation deformation occurs at both ends of the crack, and the shear fracture component increases. Blast disturbance aggravates the internal damage of the surrounding rock of the tunnel and promotes the transformation of the internal fracture of the specimen from tensile to shear.

Fig. 5 shows the distribution characteristics of the acoustic emission events RA-AF-Energy in the surrounding rock of the tunnel under the combined action of static stress loading and blasting disturbance. The tensile fracture events at low energy levels are mainly distributed in areas with low RAs, high AFs, low RAs and low AF values, while the tensile fracture events at high energy levels are mainly distributed in areas with low RAs and low AF values. Under the coupling effect of

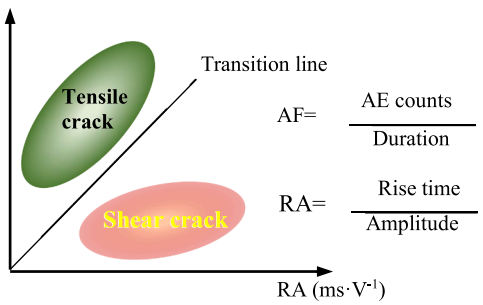

Fig. 3. AE Signal RA-AF Division Criteria.

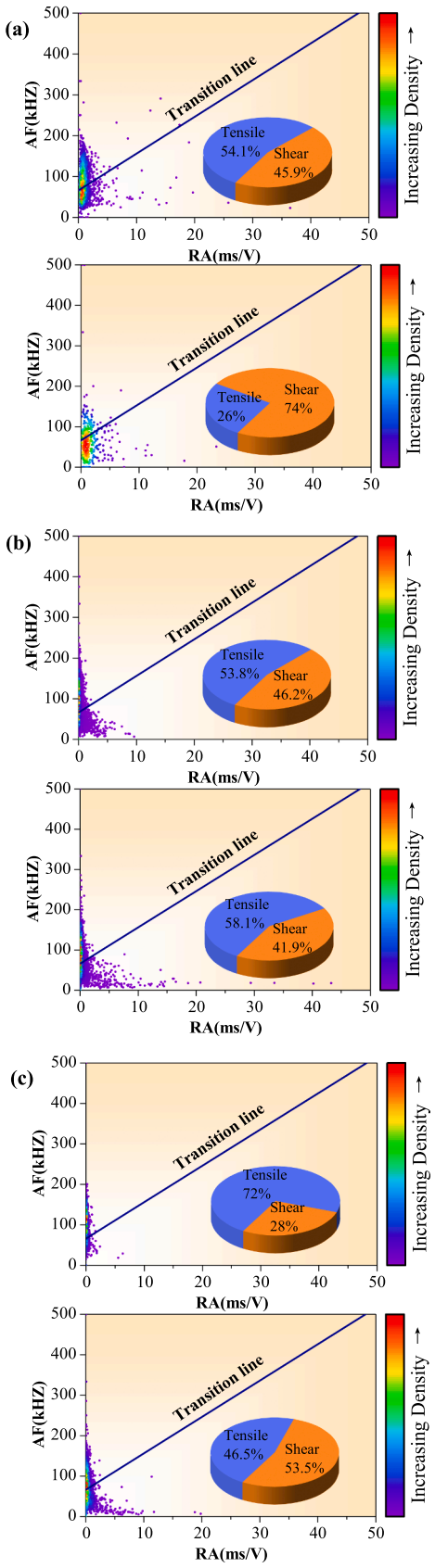

Fig. 4. Scatter density map associated with RA and AF under different blast direction: (a) Roof; (b) Sidewall; and (c) Floor.

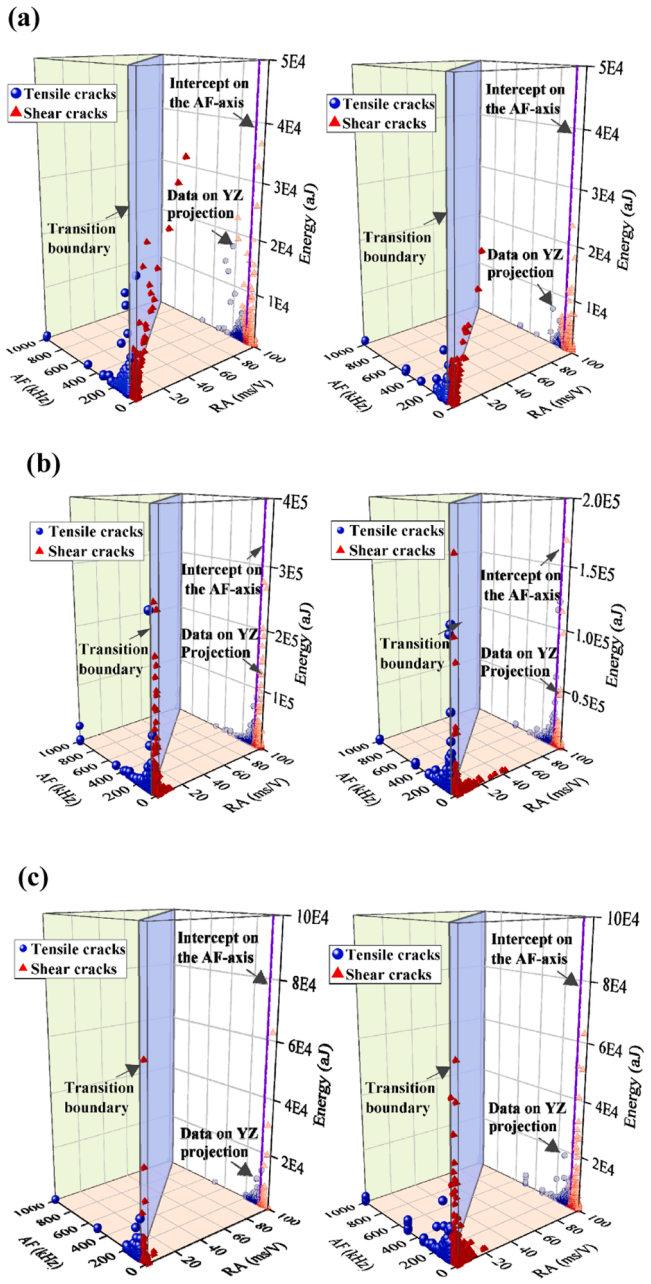

Fig. 5. Three-dimensional spatial distribution characteristics of acoustic emission signal RA-AF-Energy: (a) Roof; (b) Sidewall; and (c) Floor.

principal stress and blast disturbance, there are relatively few large energy level fracture events in the surrounding rock of the tunnel, and most of them are distributed in the shear fracture area. In addition, the number of large-level fracture events in the surrounding rock of the tunnel tends to increase during the gradual increase in damage caused by blasting disturbance, indicating that blasting disturbance promotes the penetration of internal cracks, which is consistent with the conclusion of Li et al.[48]. The fracture evolution law based on the acoustic emission energy level can be applied to the monitoring of mine rock mass stability and the prediction of dynamic disasters caused by ground pressure.

It should be noted that when the direction of blasting disturbance is

in the roof, less frequent blasting disturbance will cause tunnel damage (12 roof disturbances), and the new phenomenon of large-level shear fracture produced in this stage is not obvious. It is considered that the prestress loading results in a high stress concentration, and the blasting disturbance quickly causes local macroscopic rupture. When the expansion of the damage zone of the surrounding rock induced by blasting disturbance is mainly tensile cracks, the rock mass is relatively stable, while the final expansion and penetration of cracks require multifrequency blasting disturbance to provide external load stimulation (22 disturbances are applied to induce the penetration of cracks inside the tunnel, resulting in macroscopic cracks). When the blasting disturbance causes the shear crack to expand, the internal deformation of the rock mass is in the inelastic deformation stage, the rock mass is close to the failure threshold, and less frequent blasting disturbances can trigger internal crack penetration (such as through the roof) of the rock surrounding the tunnel. On the one hand, the difference in the regional stress concentration affects the development of deformation and cracks. On the other hand, the load excitation input of the blasting disturbance to the local area promotes the expansion and penetration of cracks in the local area.

2.3. Spatial distribution of tensile and shear cracks

In this study, the simplex positioning algorithm is used to calculate the seismic position. The algorithm has high positioning accuracy and can accurately locate and calculate the seismic position [43,44,49].

Fig. 6 displays the internal fracture distribution and fracture type distribution of the rock surrounding the tunnel under the coupling effect of static stress and blasting disturbance in different directions. During the static stress loading stage, microfracture events clustered significantly in the spandrel and arch foot areas of the tunnel. The inversion results of the fracture mechanism show that the clustering effect of tensile cracks is significant in this region, indicating that the static stress loading stage of the rock surrounding the tunnel is dominated by tensile cracks.

To quantitatively investigate the fracture response in terms of regional damage, eight regions are divided around the tunnel in this study based on the principle of equal division by area, including the roof, floor, left (right) spandrel, left (right) sidewall, and left (right) wall corner. By counting the number of tensile and shear cracks in 8 areas of the rock surrounding the tunnel, the leading types of failure in different areas of the rock surrounding the tunnel are revealed.

When the blasting disturbance comes from the roof, the proportion of tensile rupture events in the blasting side area is 31 %. When the blasting disturbance comes from the right side, the proportion of tensile rupture events in the right side area is 56.5 %. When the blasting disturbance comes from the direction of the floor, the proportion of tensile rupture events in the blasting side area is 52.2 %, as shown in Fig. 7. The blasting disturbance wave acting on the relative arc boundary of the straight sidewall will cause more reflection tensile damage, and the reflection tensile effect of the disturbance wave on the empty surface of the tunnel is significant. Therefore, the proportion of the reflected tensile wave produced by the disturbance wave on the empty surface of the straight wall is greater than that of the curved structure, and the proportion of new tensile cracks increases. Based on the distribution results of tensile and shear cracks under different blasting disturbance directions, when the blasting side is a straight sidewall, the failure of the damage area is dominated by tensile cracks, while when the blasting side is an arc structural plane, the failure of the damage area is mainly dominated by shear failure, indicating that the propagation mechanism of the surrounding rock damage zone of the tunnel is related to the shape and curvature of the structural plane of the blasting side of the tunnel. The correlation between the damage area expansion mechanism and the blasting disturbance direction is revealed. Therefore, when formulating the support type, the supporting tunnel support needs to match the failure mechanism of the mining tunnel to achieve the maximum effect.

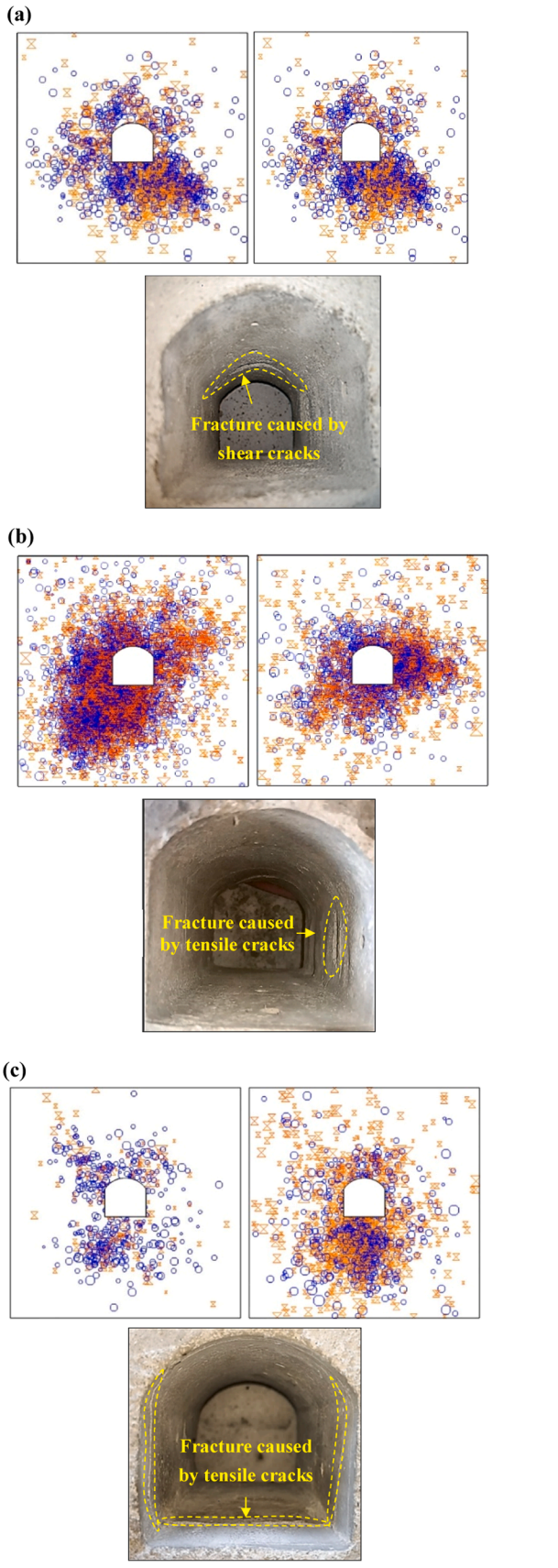

Fig. 6. Failure mechanism of tunnel under different blasting disturbance directions: (a) Roof; (b) Right sidewall; and (c) Floor.

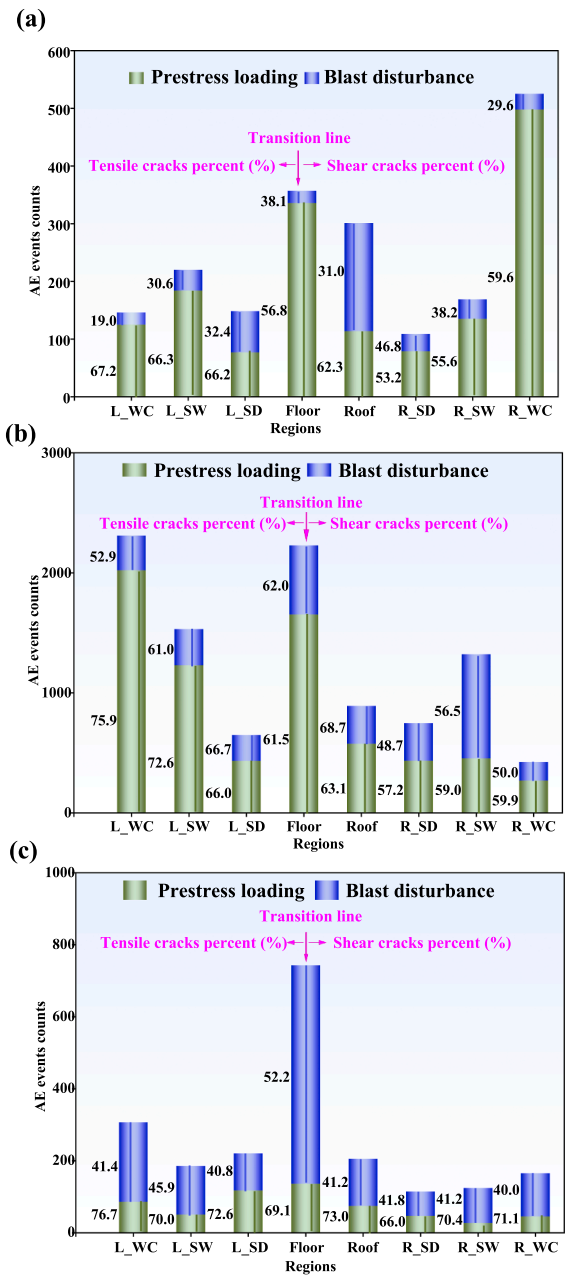

Fig. 7. The proportion of tensile and shear cracks in the surrounding rock of the tunnel in different regions under the action of disturbance waves in different directions:(a) Roof; (b) Sidewall; and (c) Floor.

In the process of the overall "tensile—shear" mode transformation of the expansion mechanism of the surrounding rock damage zone of the tunnel, the difference in the diffraction effect of the disturbance waves in different directions in the tunnel leads to the asymmetric expansion of the damage area and the differential accumulation of the damage degree. As a result, the fracture mechanism of each region of the rock surrounding the tunnel is different in the process of transformation under the action of specific frequency disturbance waves. Statistics show that each region of the rock surrounding the tunnel dominates the crack types in different stages and reveal the regional difference in the evolution mode of the fracture mechanism of the surrounding rock of the tunnel. Tensile type fracture is mainly expressed by "T", and shear type fracture is represented by "S". The main transformation modes of regional fractures in the surrounding rock of a tunnel under the effect of disturbance waves in different directions are the "T→T", "T→S" and "S→S" modes, as shown in Fig. 8. Due to the different degrees of stress concentration in different regions of the rock surrounding the tunnel under static stress loading, the regional deformation and crack development stages are different.

Due to the initial stress loading, the damage area is mainly a tensile crack, and the local area (such as the right arch foot when blasting disturbance occurs in the roof area), and under the action of multiple blasting disturbances, further deformation and crack propagation and penetration occur in the surrounding rock damage zone of the tunnel, and the crack propagation in some areas is mainly shear fracture. This observation shows that the surrounding rock deformation has developed to the stage of unstable crack propagation under the action of repeated blasting disturbance, while tensile fracture continues to be dominant in some areas, indicating that the internal deformation of the surrounding rock is still in the stage of stable growth. From the expansion results of the damage zone of the rock surrounding the tunnel under the disturbance of different blasting directions, it can be seen that the deformation and cracks in the damage zone of the rock surrounding the tunnel have further expanded under multiple blasting disturbances. A change in the disturbance direction not only leads to a difference in the amount of crack propagation in different regions of the rock surrounding the tunnel but also leads to a differential transformation of the tunnel propagation mechanism.

3. Numerical calculation model and analysis of results

3.1. Model setting

The Sishanling Iron Mine is located in Benxi City, Liaoning Province, China. It employs the sublevel stoping with subsequent backfilling method for mining operations. The initial mining levels are at −960 m and −1020 m. Each sublevel has a height of 60 m, and the mining drifts within the scope measure 5.4 m in width and 5.1 m in height. At the −1020 m sublevel, the horizontal stress is approximately 37.8 MPa, while the vertical stress is approximately 23.6 MPa.

To investigate the mechanism of drift fracture under different blasting disturbance directions, a two-dimensional model measuring 60 m in width and height was developed, as shown in Fig. 9. To reduce the dependence of crack propagation on the grid size in the rock surrounding the tunnel under dynamic and static loads, the dynamic crack propagation process in the damaged area can be effectively investigated, the grid in the area near the tunnel can be refined, the block size in the area far from the tunnel can be enlarged, and the consumption of calculations can be reduced.

The peak intensity of the designed disturbance waveform is 20 MPa, and two dynamic disturbances are implemented. The dynamic load calculation time for each time is 0.07 s (Fig. 10), and the disturbance waveform frequency is set to 650 Hz (λ/D=1.27).

The disturbance mechanism of stress waves at the tunnel involves stress adjustment and fracture response induced by the diffraction effect of the waves at the tunnel. When the ratio of the stress wave wavelength to the hole length (λ/D) is less than 1/1000, the diffraction phenomenon is negligible; when the ratio is between 1/100 and 1/10, the diffraction phenomenon becomes significant; when the ratio equals or exceeds 1, the diffraction transitions into scattering; when the ratio approaches 0, i.e., as the diameter of the diffraction hole increases, the diffraction phenomenon gradually diminishes [50,51]. The frequency of the waveforms generated by indoor blasting disturbances is relatively high, specifically 54 kHz, resulting in a wavelength-to-tunnel-span ratio of $\lambda/D = 1.27$. To ensure the similarity of the diffraction effect of the shock wave at the tunnel, i.e., to maintain an equivalent ratio of the disturbance wave wavelength to the tunnel span, the frequency of each stress disturbance wave is set to 650 Hz, yielding a corresponding $\lambda/D = 1.27$.

The study considers only far-field disturbance stresses and excludes the influence of detonation gases on tunnel rupture. In addition, when

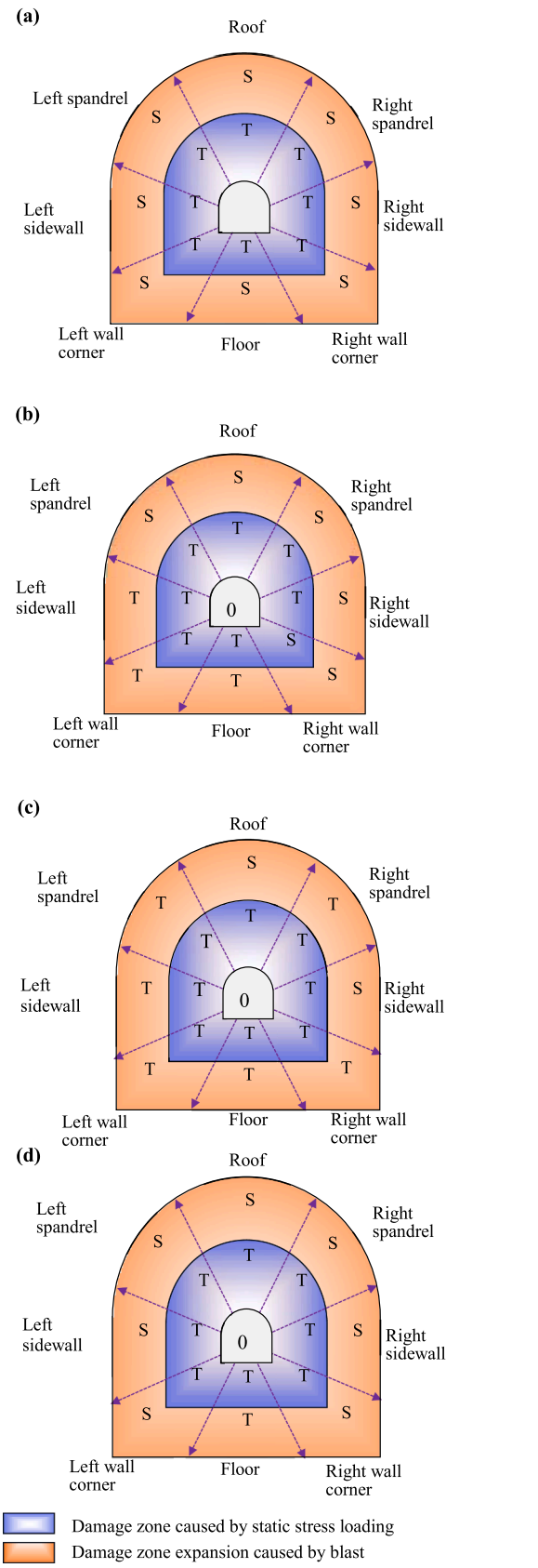

Fig. 8. Regional evolution of dominant microcracks types under varying blasting direction: (a) Roof; (b) Right spandrel; (c) Right wall corner; and (d) Floor.

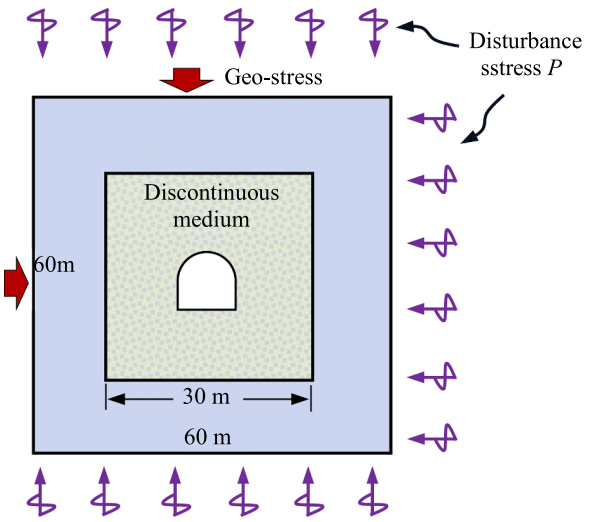

Fig. 9. Model size and boundary conditions.

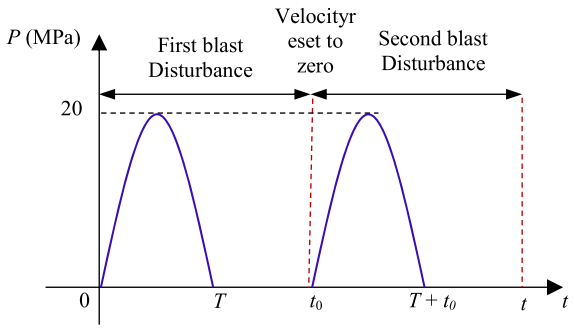

Fig. 10. Disturbance waveform setting.

the peak value of the disturbance wave is significantly lower than the failure strength and applied to the model, the rate of increase in stress and strain within the rock mass remains relatively small. According to Li et al.[52], when the amplitude of the stress wave is less than 60 % of the static strength of the rock (mass), the internal damage under disturbance is minimal and can be disregarded. Consequently, numerical simulations amplify the intensity of the disturbance wave. Although the single disturbance effect exceeds actual conditions, the fracture propagation mode within the surrounding rock remains similar, providing insight into the expansion mechanism of the damage zone in the tunnel's surrounding rock under mining-induced stress.

After the first dynamic load, the internal velocity of the model is reset to zero to achieve the stress equilibrium state after the disturbance. The specific block calculation parameters are shown in Table 1 below [53].

3.2. *Model results analysis*

When the principal stress direction of the rock mass is horizontal, the excavation unloading effect causes the spatial shape of the excavation damage zone of the surrounding rock mass of the tunnel to be "vertical elliptic". Shear cracks are mainly distributed in the roof and floor of the tunnel, and tensile cracks are mainly distributed on the two sides of the tunnel, as shown in Fig. 11. After the rock mass in the principal stress direction is instantly removed from the radial stress direction, the shallow rock mass lacks reverse constraints, and radial deformation occurs, which leads to tensile cracks in the area in the principal stress direction. In the region of the vertical principal stress direction, the

Table 1
Block and joint parameters of the model.

Rock mass				Contact	
Attributes	Target value	Checking value	Error (%)	Attributes	Checking value
Young's modulus (GPa)	50.2	52.6	5	Normal stiffness (GN/m)	430
UCS (MPa)	17.8	17.6	1.1	Shear sitffness (GN/m)	130
				Cohesion (MPa)	10
				Friction angle (°)	20
				UTS(MPa)	0.001

stress is relatively concentrated due to the deflection of the stress, which leads to shear cracks in the rock mass. In addition, under the effect of a blast disturbance wave, the internal damage to the rock surrounding the tunnel is further aggravated, and the number and length of cracks increase. The number and type of cracks propagating within the surrounding rock of the tunnel under blasting disturbance in different directions differ. For example, the blasting disturbance in the roof direction induces a significant expansion of the damage zone in the roof of the tunnel, while the expansion degree of the damage zone in the two sides of the tunnel is relatively small. When the disturbance wave comes from the right side of the tunnel, the damage area of the roof and floor is expanded, and the cracks in the free surface area of the right side are obviously penetrated. When the disturbance comes from the floor, the damage area of the tunnel floor expands obviously, and the position of the free surface is obviously connected. The disturbance in different directions induces the differential expansion and penetration of the damage zone in the excavation of the rock surrounding the tunnel. For example, the penetration degree of cracks on the blasting side of a tunnel induced by a roof dynamic disturbance is less than that on the right side and by a floor disturbance, which shows that the diffraction effects of stress waves in different directions are different on the empty surface of a tunnel. This leads to a difference in the penetration degree between cracks. This phenomenon verifies the difference in crack types caused by different structural plane curvatures of the tunnel and shows that the penetration of cracks easily occurs on the empty surface of the straight sidewall of the tunnel, so the proportion of reflected tensile waves caused by cracks is relatively high. Therefore, in view of the differences in the expansion position and fracture mechanism of the damage zone caused by blasting disturbance stress waves in different directions, tunnel support should focus on strengthening the tensile sheet failure in the straight sidewall area of the tunnel and controlling the deformation caused by the expansion of the fragmentation block. The support depth should be lengthened in the vertical principal stress direction to reduce the gradual expansion of the damage area under the action of frequent blasting disturbance.

When blasting disturbance promotes the mutual expansion of cracks until they are connected, there will be spalling in the shallow area of the surrounding rock of the tunnel, as shown in Fig. 12. First, cracks in the rock surrounding the tunnel initiates but does not penetrate any macroscopic fractures around the tunnel after excavation unloading; however, they are well developed under repeated blast disturbances. For example, when the blasting disturbance wave comes from the right side

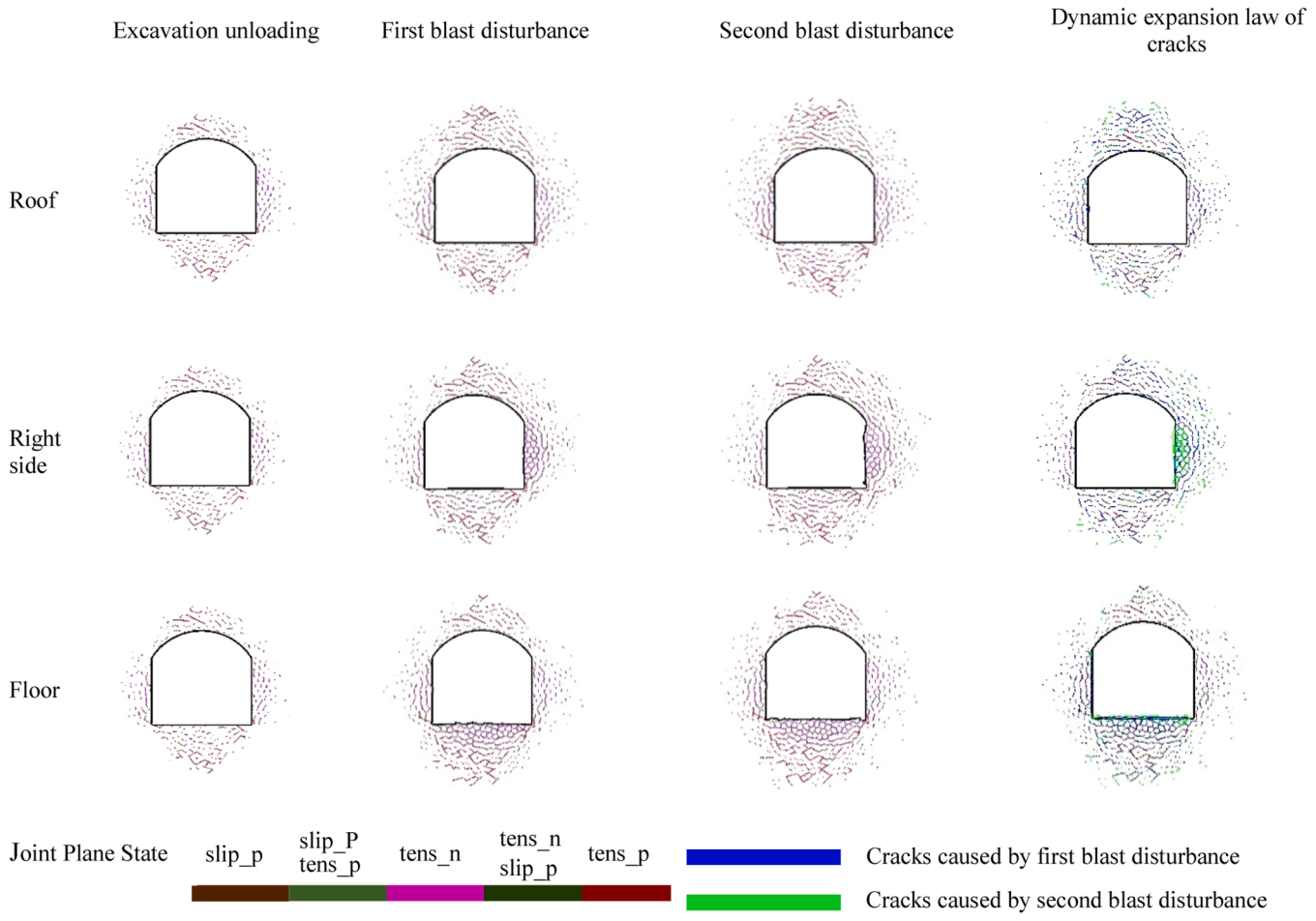

Fig. 11. Microcracks distributions triggered by blast disturbance from varying directions.

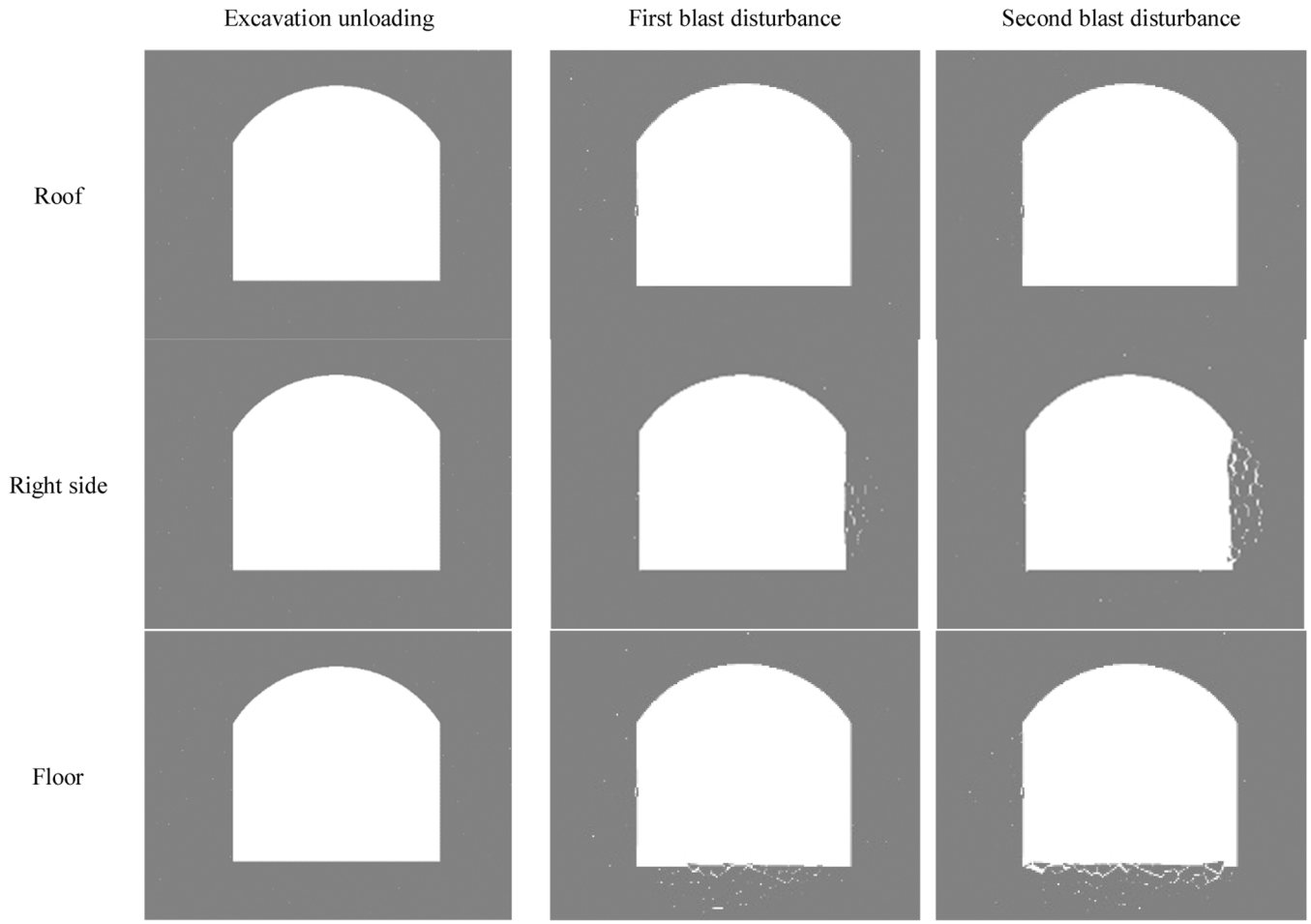

Fig. 12. Macro-fracture mode of tunnel under blasting disturbance in different directions.

and floor of the tunnel, an obvious crack penetration zone appears in the area facing the blasting side of the tunnel, and the degree of penetration and rupture is aggravated under multiple disturbances. In addition, the degree of macroscopic fracture of the tunnel induced by disturbance waves in different directions is different. For example, when the blasting disturbance comes from the roof, the degree of macroscopic fracture of the cracks caused by the blasting disturbance is low, and there is no obvious block spalling; when the blasting disturbance direction is on the right side or roof of the tunnel, significant spalling damage occurs in the area on the blast side of the tunnel. The results show that the mechanical and fracture responses to blasting disturbances in different directions are different due to the different structural curvatures of the blasting side.

4. Discussion

Study reveals that tensile cracks, shear cracks, and mixed-mode cracks exhibit distinct mechanical behaviors and propagation paths, resulting in significantly different macroscopic failure patterns across various regions of the tunnel. For example, in the roof area, unloading under high confining pressure tends to induce tensile crack development, which rapidly propagates along primary fractures, causing delamination and spalling of layered rock masses. Conversely, in the sidewall region, the superposition of tectonic stress and mining-induced stress facilitates shear crack sliding along weak planes, potentially leading to overall outward bulging or sliding instability. This differential failure mechanism requires support design to be dynamically tailored to the type and spatial distribution of cracks: for tensile-dominated zones, enhancing tensile resistance is critical; for shear-sliding zones, rigid support elements should be employed to dissipate shear energy and preserve the residual strength of the surrounding rock. Through laboratory experiments and numerical simulations, this study has established a clear correlation framework linking crack type, failure mode, and support parameters, offering a theoretical foundation for the refined design of tunnel support.

5. Conclusion

By conducting experimental investigations and numerical simulation studies on rock fractures surrounding tunnels induced by blasting disturbances in different directions, in this paper we analyze the distribution and expansion patterns of microcracks in rock surrounding tunnels induced by disturbance waves from roofs, floors and sidewalls of tunnels and revealed the mechanism of tunnel fracture caused by disturbance waves in different directions. The following conclusions can be drawn:

(1) The AE signal changes from a high AF and low RA to a low AF and high RA during the coupling effect of static stress and blast disturbance. Among them, the internal micropores are gradually compacted during the static stress loading stage, mainly tensile fracture. The blasting disturbance promotes the expansion of internal cracks, and shear cracks are the main stage of penetration.
(2) The difference in the curvature of the free surface on the blast-facing side of the tunnel affects the reflection and tensile effect of the disturbance wave at the tunnel. Compared with disturbance waves in the direction of the roof, disturbance waves in the direction of the sidewall or floor will induce more tensile cracks in the area on the blast side of the tunnel, and the reflected

stretching effect of the disturbance waves is significant. The difference in the diffraction effect of disturbance waves in different directions in the tunnel causes asymmetric expansion of the damaged area and differential accumulation of damage. The fracture mechanism of each area of the rock surrounding the tunnel shows differences in the "tensile—shear" transition process.

(3) Disturbance waves in different directions induce different expansions of the damage zone of surrounding rock excavation, which leads to different macrofailure modes. The degree of penetration between cracks in the area facing the explosion caused by the dynamic disturbance waves in the right side and floor direction is greater than that in the roof direction, which can easily trigger macroscopic rupture in the shallow area on the side of the tunnel facing the explosion.

CRediT authorship contribution statement

Jianpo Liu: Writing – review & editing, Supervision, Methodology, Funding acquisition, Conceptualization. **Fengtian Li:** Writing – review & editing, Writing – original draft, Investigation. **Xiaonan Wang:** Visualization, Resources. **Yingtao Si:** Writing – review & editing, Data curation. **Yandi Fan:** Visualization, Data curation. **Zixuan Zhang:** Visualization, Validation. **Yongxin Wang:** Validation.

Declaration of Competing Interest

The authors declare that they have no known competing interests or personal relationships that could have appeared to influence the work reported in this paper.

Acknowledgements

This work was financially supported by the National Key Research and Development Program of China (2023YFC2907204) and the National Natural Science Foundation of China (52174142) and the Science and Technology Program of Liaoning Province (2023JH1/10400004).

References

[1] L.Z. Tang, Y. Chen, C. Wang, et al., Dynamic properties of rock disturbed frequently dynamically in process of unloading under high static stress, Chin. J. Nonferrous Met. 26 (8) (2016) 1728–1736, https://doi.org/10.19476/j.ysxb.1004.0609.2016.08.016.

[2] W.C. Zhu, Y.J. Zuo, S.M. Shang, et al., Numerical Simulation of instable failure of deep rock tunnel triggered by dynamic disturbance, Chin. J. Rock Mech. Eng. 5 (2007) 915–921.

[3] L. Weng, X.B. Li, M. Tao, Influence of geostress orientation on fracture response of deep underground cavity subjected to dynamic loading, Shock Vib. (2015) 1–9, https://doi.org/10.1155/2015/575879.

[4] W.T. Liu, Y.H. Du, Y.B. Liu, et al., Failure characteristics of floor mining-induced damage under deep different dip angles of coal seam, Geotech. Geol. Eng. 37 (2) (2019) 985–994, https://doi.org/10.1007/s10706-018-0666-9.

[5] G.X. Chen, L.M. Dou, M.S. Gao, et al., Numerical simulation of dynamic vibration affecting rock burst in mining gateway caused by tremor, Chin. J. Min. Saf. Eng. 26 (2) (2009) 153–157.

[6] J.C. Gu, A.M. Chen, J.M. Xu, et al., Model test study of failure patterns of anchored tunnel subjected to explosion load, Chin. J. Rock Mech. Eng. 5 (2008) 1315–1320.

[7] J. Shen, J.C. Gu, A.M. Chen, et al., Development and applications of the model test apparatus on anti-explosion structures geotechnical engineering, Chin. J. Undergr. Sp. Eng. 6 (2007) 1077–1080.

[8] M. Tao, H.T. Zhao, X.B. Li, et al., Failure characteristics and stress distribution of pre-stressed rock specimen with circular cavity subjected to dynamic loading, Tunn. Undergr. Sp. Tech. 81 (2018) 1–15, https://doi.org/10.1016/j.tust.2018.06.028.

[9] J.D. Qiu, X.B. Li, D.Y. Li, et al., Physical model test on the deformation behavior of an underground tunnel under blasting disturbance, Rock Mech. Rock Eng. 54 (1) (2021) 91–108, https://doi.org/10.1007/s00603-020-02249-2.Aggelis. DG (2011) Classification of cracking mode in concrete by acoustic emission parameters. Mech Res Commun 38:153–157, ⟨https://doi.org/10.1016/j.mechrescom.2011.03.007⟩.

[10] P. Xu, R.S. Yang, J.J. Zuo, et al., Research progress of the fundamental theory and technology of rock blasting, Int. J. Miner. Metall. Mater. 29 (4) (2022) 705–716, https://doi.org/10.1007/s12613-022-2464-x.Aggelis. DG, Mpalaskas AC, Matikas TE (2013) Acoustic signature of different fracture modes in marble and cementitious materials under flexural load. Mech Res Commun 47:39–43, ⟨https://doi.org/10.1016/j.mechrescom.2012.11.007⟩.

[11] Y.R. Xue, X.Q. He, D.Z. Song, et al., Energy evolution and structural health monitoring of coal under different failure modes: An experimental study, Int. J. Miner. Metall. Mater. 31 (5) (2024) 917–928, https://doi.org/10.1007/s12613-024-2822-y.

[12] X.B. Li, J.D. Qiu, Y.Z. Zhao, et al., Instantaneous and long-term deformation characteristics of deep room-pillar system induced by pillar recovery, T. Nonferr. Met. Soc. 30 (10) (2020) 2775–2791, https://doi.org/10.1016/S1003-6326(20)65420-6.

[13] J.P. Liu, S.D. Xu, Y.H. Li, et al., Analysis of Rock Mass Stability Based on Mining-Induced Seismicity: A Case Study at the Hongtoushan Copper Mine in China, Rock Mech. Rock Eng. 52 (1) (2019) 265–276, https://doi.org/10.1007/s00603-018-1541-y.

[14] T. Li, X.T. Feng, R. Wang, et al., Characteristics of rockburst location deflection and its microseismic activities in a deep tunnel, Rock Soil Mech. 40 (7) (2019) 2847–2854, https://doi.org/10.16285/j.rsm.2018.0470.

[15] X.T. Feng, J.P. Liu, B.R. Chen, et al., Monitoring, warning, and control of rockburst in deep metal mines, Eng. -PRC 3 (4) (2017) 538–545, https://doi.org/10.1016/J.ENG.2017.04.013.

[16] J.Q. Jiang, X.T. Feng, C.X. Yang, et al., Experimental study on the failure characteristics of granite subjected to weak dynamic disturbance under different σ3 conditions, Rock Mech. Rock Eng. 54 (11) (2021) 5577–5590, https://doi.org/10.1007/s00603-021-02542-8.

[17] G. Lei, S.Y. Zhu, X.Z. Shi, et al., The spatio-temporal evolution of rock failure due to blasting under high stress, Appl. Sci. -Basel 13 (5) (2023) 2781, https://doi.org/10.3390/app13052781.

[18] X.H. Li, Z.M. Zhu, M. Wang, et al., Influence of blasting load directions on tunnel stability in fractured rock mass, J. Rock Mech. Geotech. Eng. 14 (2) (2022) 346–365, https://doi.org/10.1016/j.jrmge.2021.06.010.

[19] H.L. Liu, L.Q. Huang, Z.W. Wang, et al., Experimental study on dynamic response of hard rock blasting under in-situ stress, Int. J. Rock Mech. Min. Sci. 182 (2024) 105860, https://doi.org/10.1016/j.ijrmms.2024.105860.

[20] Y.X. Wang, M.M. He, Numerical investigation on effect of inclination and position of structural planes on rockbursts triggered by blasting disturbance in deep-buried tunnels, Rock Mech. Rock Eng. 58 (3) (2025) 2739–2761, https://doi.org/10.1007/s00603-024-04314-6.

[21] J.W. Zhang, D.Y. Wan, W.T. Gao, et al., Numerical study on the dynamic propagation model of cracks from different angles under the effect of circular hole explosion, Appl. Sci. -Basel 13 (13) (2023) 7955, https://doi.org/10.3390/app13137955.

[22] T. Zhang, Y.Y. Xu, C. Wei, et al., The influence of disturbance location and intensity on the deformation and failure of deep roadway surrounding rocks, Front. Mater. 12 (2025) 1550247, https://doi.org/10.3389/fmats.2025.1550247.

[23] Z. Zheng, S.X. Li, Q. Zhang, et al., True triaxial test and DEM simulation of rock mechanical behaviors, meso-cracking mechanism and precursor subject to underground excavation disturbance, Eng. Geol. 337 (2024) 107567, https://doi.org/10.1016/j.enggeo.2024.107567.

[24] Z. Zheng, H.Y. Xu, K. Zhang, et al., Intermittent disturbance mechanical behavior and fractional deterioration mechanical model of rock under complex true triaxial stress paths, Int. J. Min. Sci. Technol. 34 (1) (2024) 117–136, https://doi.org/10.1016/j.ijmst.2023.11.007.

[25] J. Zhao, G.M. Zhao, X.R. Meng, et al., Mechanism of surrounding rock failure in impact stress and in-situ stress in circular tunnel, Geomech. Geophys. Geo-Energy Geo-Resour. 9 (1) (2023) 165, https://doi.org/10.1007/s40948-023-00709-x.

[26] C.Q. Chu, S.C. Wu, C.J. Zhang, et al., Microscopic damage evolution of anisotropic rocks under indirect tensile conditions: Insights from acoustic emission and digital image correlation techniques, Int. J. Miner. Metall. Mater. 30 (9) (2023) 1680–1691, https://doi.org/10.1007/s12613-023-2649-y.

[27] S.Y. Ouyang, Y.L. Huang, N. Zhou, et al., Experiment on acoustic emission response and damage evolution characteristics of polymer-modified cemented paste backfill under uniaxial compression, Int. J. Miner. Metall. Mater. 30 (8) (2023) 1502–1514, https://doi.org/10.1007/s12613-023-2617-6.

[28] T.Z. Zhang, H.G. Ji, X.B. Su, et al., Evaluation and classification of rock heterogeneity based on acoustic emission detection, Int. J. Miner. Metall. Mater. 29 (12) (2022) 2117–2125, https://doi.org/10.1007/s12613-021-2381-4.

[29] J.P. Liu, Z.S. Liu, S.Q. Wang, et al., Analysis of acoustic emission source mechanisms for tensile and shear cracks of rock fractures, J. Northeast. Univ. 36 (11) (2015) 1624–1628.

[30] J.P. Liu, Y.H. Li, S.D. Xu, et al., Cracking mechanisms in granite rocks subjected to uniaxial compression by moment tensor analysis of acoustic emission, Theor. Appl. Fract. Mec. 75 (2015) 151–159, https://doi.org/10.1016/j.tafmec.2014.12.006.

[31] J.P. Liu, Y.H. Li, S.D. Xu, et al., Moment tensor analysis of acoustic emission for cracking mechanisms in rock with a pre-cut circular hole under uniaxial compression, Eng. Fract. Mech. 135 (2015) 206–218, https://doi.org/10.1016/j.engfracmech.2015.01.006.

[32] J.P. Liu, Y.H. Li, S.D. Xu, Estimation of cracking and damage mechanisms of rock specimens with precut holes by moment tensor analysis of acoustic emission, Int. J. Fract. 188 (1) (2014) 1–8, https://doi.org/10.1007/s10704-014-9940-x.

[33] D.G. AGGELIS, Classification of cracking mode in concrete by acoustic emission parameters, Mech. Res. Commu 38 (3) (2011) 153–157, https://doi.org/10.1016/j.mechrescom.2011.03.007.

[34] JCMS B5706, Monitoring method for active cracks in concrete by acoustic emission, Japan: Federation of Construction Materials Industries, Japan, 2003.

[35] M. OHTSU, Y. TOMODA, Phenomenological model of corrosion on process in reinforced concrete identified by acoustic emmission, Acids Mater. J. 105 (2) (2008) 194–199.
[36] K. OHNO, M. OHTSU, Crack classification in concrete based on acoustic emission, Constr. Build. Mater. 24 (12) (2010) 2339–2346, https://doi.org/10.1016/j.conbuildmat.2010.05.004.
[37] C. Liu, S.Y. Yin, J. Zhang, et al., Acoustic emission and energy evolution of sandstone failure subjected to deep mining stress, Chin. J. Min. Saf. Eng. 39 (3) (2022) 470–479, https://doi.org/10.13545/j.cnki.jmse.2020.0643.
[38] D.G. Aggelis, A.C. Mpalaskas, D. Ntalakas, et al., Effect of wave distortion on acoustic emission characterization of cementitious materials, Constr. Build. Mater. 35 (2012) 183–190, https://doi.org/10.1016/j.conbuildmat.2012.03.013.
[39] H.J. Wang, D.A. Liu, Z.D. Cui, et al., Investigation of the fracture modes of red sandstone using XFEM and acoustic emissions, Theor. Appl. Fract. Mec. 28 (2016) 189–190, https://doi.org/10.1016/j.tafmec.2016.03.012.
[40] A. Farhidzadeh, A.C. Mpalaskas, T.E. Matikas, et al., Fracture mode identification in cementitious materials using supervised pattern recognition of acoustic emission features, Constr. Build. Mater. 67 (2014) 129–138, https://doi.org/10.1016/j.conbuildmat.2014.05.015.
[41] K. Du, X.F. Li, M. Tao, et al., Experimental study on acoustic emission (AE) characteristics and crack classification during rock fracture in several basic lab tests, Int. J. Rock Mech. Min. Sci. 133 (2020) 104411.
[42] Y.T. Si, J.P. Liu, F.T. Li, et al., Experimental and theoretical investigation of roadway fracture induced by static-blast loading using acoustic emission, Eng. Fail. Anal. 143 (2023) 106909, https://doi.org/10.1016/j.engfailanal.2022.106909.
[43] J.P. Liu, C.Y. Zhang, Y.T. Si, et al., Temporal-spatial evolution of acoustic emission during progressive fracture processes around tunnel triggered by blast-induced disturbances under uniaxial and biaxial compression, Tunn. Undergr. Sp. Tech. 96 (2020) 103229, https://doi.org/10.1016/j.tust.2019.103229.
[44] J.P. Liu, S.D. Xu, Y.H. Li, et al., Studies of AE time-space evolution characteristics during failure process of rock specimens with prefabricated holes, Chin. J. Rock Mech. Eng. 31 (12) (2012) 2538–2547.
[45] Y.X. Gan, S.C. Wu, Y. Ren, et al., Evaluation indexes of granite splitting failure based on RA and AF of AE parameters, Rock Soil Mech. 41 (7) (2020) 2324–2332, https://doi.org/10.16285/j.rsm.2019.1460.
[46] D.G. Aggelis, A.C. Mpalaskas, T.E. Matikas, Acoustic signature of different fracture modes in marble and cementitious materials under flexural load, Mech. Res. Commu 47 (2013) 39–43, https://doi.org/10.1016/j.mechrescom.2012.11.007.
[47] Y.T. Si, J.P. Liu, K.K. Hou, et al., Roadway fracture mechanism investigation subjected to static and blast loading under different lateral pressure coefficients, Eng. Fract. Mech. 292 (2023) 109663, https://doi.org/10.1016/j.engfracmech.2023.109663.
[48] Y.H. Li, J.P. Liu, X.D. Zhao, et al., Study on b-value and fractal dimension of acoustic emission during rock failure process, 2574, Rock Soil Mech. 30 (9) (2009) 2559–2563, https://doi.org/10.16285/j.rsm.2009.09.028.
[49] S.D. Xu, T.X. Chen, J.Q. Liu, et al., Exponential decay law of acoustic emission and microseismic activities caused by disturbances associated with multilevel loading and mining blast, T. Nonferr. Met. Soc. 31 (11) (2021) 3549–3563, https://doi.org/10.1016/S1003-6326(21)65747-3.
[50] X. Wang, M. Cai, Influence of wavelength-to-excavation span ratio on ground motion around deep underground excavations, Tunn. Undergr. Space Technol. 49 (B12) (2015) 438–453.
[51] Z.R. Zheng, W.Z. Wui, A.H. Li, Optics, Harbin Institute of Technology Press, 2015.
[52] X.B. Li, T.S. Lok, J. Zhao, Dynamic characteristics of granite subjected to intermediate loading rate, Rock Mech. Rock Eng. 38 (1) (2005) 21–39.
[53] Y.T. Si, J.P. Liu, F.T. Li, et al., Zhang, Roadways fracture response under varying dominant blasting frequencies and lateral pressure coefficients, Int. J. Impact Eng. 181 (2023) 104761.

Dr. Jianpo Liu is a professor at State Key Laboratory of Intelligent Deep Metal Mining and Equipment, Northeastern University. Research focus on rock mass mechanics in deep metal mining environments, monitoring and mitigation of deep ground pressure disasters, and microseismic/acoustic emission monitoring technologies.